



**HAL**  
open science

# The geometry of the generalized gamma manifold and an application to medical imaging

Sana Rebbah, Florence Nicol, Stéphane Puechmorel

► **To cite this version:**

Sana Rebbah, Florence Nicol, Stéphane Puechmorel. The geometry of the generalized gamma manifold and an application to medical imaging. *Mathematics*, 2019, 7 (8), pp.art. no. 674. 10.3390/math7080674. hal-02159244

**HAL Id: hal-02159244**

**<https://enac.hal.science/hal-02159244>**

Submitted on 18 Jun 2019

**HAL** is a multi-disciplinary open access archive for the deposit and dissemination of scientific research documents, whether they are published or not. The documents may come from teaching and research institutions in France or abroad, or from public or private research centers.

L'archive ouverte pluridisciplinaire **HAL**, est destinée au dépôt et à la diffusion de documents scientifiques de niveau recherche, publiés ou non, émanant des établissements d'enseignement et de recherche français ou étrangers, des laboratoires publics ou privés.

Article

# The geometry of the generalized gamma manifold and an application to medical imaging

Sana Rebbah <sup>1</sup> , Florence Nicol <sup>2</sup> and Stéphane Puechmorel <sup>3,\*</sup>, for the Alzheimer's Disease Neuroimaging Initiative\*

<sup>1</sup> ENAC and INSERM ToNIC, Université de Toulouse; sana.rebbah@inserm.fr

<sup>2</sup> ENAC, Université de Toulouse, florence.nicol@enac.fr

<sup>3</sup> ENAC, Université de Toulouse, stephane.puechmorel@enac.fr

\* Correspondence: stephane.puechmorel@enac.fr; Tel.: +33-5-62259503

Version June 18, 2019 submitted to Mathematics

**Abstract:** The Fisher information metric provides parameterized probability densities with a Riemannian manifold structure, yielding the so-called information geometry. The information geometry of the gamma manifold associated to the family of gamma distributions has been well studied. However, only a few results are known for the generalized gamma family, that adds an extra shape parameter. The present article gives some new results about the generalized gamma manifold. This paper also introduces an application in medical imaging that is the classification of Alzheimer's disease population. In the medical field, over the past two decades, a growing number of quantitative image analysis techniques have been developed, including histogram analysis, which is widely used to quantify the diffuse pathological changes of some neurological diseases. This method presents several drawbacks. Indeed, all the information included in the histogram is not used and the histogram is an overly simplistic estimate of a probability distribution. Thus, in this study we present how using information geometry and the generalized gamma manifold improved the performance of the classification of Alzheimer's disease population.

## 1. Introduction

The generalized gamma distribution was introduced in [1], and can be viewed as a special case of the Amoroso distribution [2] in which the location parameter is dropped [3]. Apart from the gamma distribution, it generalizes also the Weibull distribution and is of common use in survival models. The purpose of the present work is to investigate some information geometric properties of the generalized gamma family, especially when restricted to the gamma submanifold. First, in Section 2, the Fisher information as a Riemannian metric and results in the case of the gamma manifold will be briefly introduced. Next, the case of the generalized gamma manifold will be detailed, using an approach based on diffeomorphism groups. In section 4, the extrinsic curvature of the gamma submanifold will be computed. Finally, an example of application in the medical imaging domain will be given in the last section.

## 2. Information geometry and the gamma manifold

Information geometry deals with parameterized families of distributions whose parameters are understood as local coordinates on a manifold and provided with a Riemannian structure by the

---

\*Data used in the preparation of this article were obtained from the Alzheimer's Disease Neuroimaging Initiative (ADNI) database ([adni.loni.ucla.edu](http://adni.loni.ucla.edu)). As such, the investigators within the ADNI contributed to the design and implementation of ADNI and/or provided data but did not participate in analysis or writing of this report. A complete listing of ADNI investigators can be found at: [http://adni.loni.ucla.edu/wp-content/uploads/how\\_to\\_apply/ADNI\\_Acknowledgement\\_List.pdf](http://adni.loni.ucla.edu/wp-content/uploads/how_to_apply/ADNI_Acknowledgement_List.pdf)

28 Fisher metric. In the sequel,  $\Theta$  will be a smooth manifold and  $(p_\theta), \theta \in \Theta$  a family of probability  
 29 density functions defined on a common event space  $\Omega$  and depending smoothly on the parameters  $\theta$ .  
 30 Thorough the paper, the Einstein summation convention on repeated indices will be used.

**Definition 1.** *The Fisher information metric on  $\Theta$  is defined at point  $\theta \in \Theta$  by the symmetric order 2 tensor:*

$$g = g_{ij} d\theta^i \otimes d\theta^j$$

where:

$$g_{ij} = E_{p_\theta} [\partial_{\theta_i} l \partial_{\theta_j} l], \quad l(\theta) = \log p_\theta$$

When the support of the density functions  $p_\theta$  does not depend on  $\theta$ , the information metric can be rewritten as:

$$g_{ij} = -E_{p_\theta} [\partial_{\theta_i} \partial_{\theta_j} l] \quad (1)$$

31 It gives rise to a Riemannian metric on  $\Theta$ .

32 When the underlying event space  $\Omega$  is also a smooth manifold, the Fisher metric has a classical  
 33 nice invariance property, that corresponds to information preservation by sufficient statistics:

34 **Proposition 1.** *Let  $\tilde{\Omega}$  be a smooth manifold and  $\Phi: \Omega \rightarrow \tilde{\Omega}$  be a smooth diffeomorphism. Let  $\tilde{g}$  be the Fisher  
 35 information metric associated to the image family  $\Phi_* p_\theta$  defined on the event space  $\tilde{\Omega}$ . Then  $\tilde{g} = g$ .*

The Fisher metric has a very simple expression when the parameterized family  $p_\theta$  is of natural exponential type. In such a case, assuming for the sake of simplicity that  $\Theta$  and  $\Omega$  are open subsets of finite dimensional real vector spaces, the density function  $p_\theta$  can be written as:

$$p_\theta(x) = \exp(\langle \theta, F(x) \rangle - \phi(\theta) + g(x)) \quad (2)$$

The function  $\phi$  in eq. 2 is called the potential function of the density and an immediate application of the definition (1) yields for the expression of the Fisher information metric:

$$g_{ij}(\theta) = \frac{\partial^2 \phi}{\partial \theta_i \partial \theta_j}(\theta) \quad (3)$$

36 A manifold with such a Riemannian metric is referred to as a Hessian structure [4]. Many  
 37 important tools from Riemannian geometry, like the Levi-Civita connection, are greatly simplified  
 38 within this frame. In the sequel, all partial derivatives  $\partial_{\theta_i}$  will be abbreviated by  $\partial_i$ .

**Proposition 2.** *For a parameterized density family  $p_\theta, \theta \in \Theta$  pertaining to the natural exponential class with potential function  $\Psi$ , the Christoffel symbols of the first kind of the associated Hessian structure are given by [5]:*

$$\Gamma_{ijk} = \frac{1}{2} \partial_i \partial_j \partial_k \phi$$

39 The gamma distribution can be written as a natural exponential family on two parameters  $(\alpha, \lambda)$ ,  
 40 defined on the parameter space  $\mathbb{R}^{+*} \times \mathbb{R}^{+*}$  by:

**Definition 2.** *The gamma distribution is the probability law on  $\mathbb{R}^{+*}$  with density relative to the Lebesgue measure given by:*

$$p(x; \alpha, \lambda) = \frac{1}{\Gamma(\lambda) \alpha^\lambda} x^{\lambda-1} e^{-\frac{x}{\alpha}}, \quad x > 0 \quad (4)$$

41 with parameters  $\alpha > 0, \lambda > 0$ .

42 The next proposition comes directly from the definition:

43 **Proposition 3.** *The gamma distribution defines a natural exponential family with natural parameters  $\lambda$  and*  
 44  *$\eta = \alpha^{-1}$  and potential function  $\phi(\eta, \lambda) = \log(\Gamma(\lambda)) - \lambda \log(\eta)$ .*

Using 3, the Fisher metric is obtained by a straightforward computation:

$$g(\eta, \lambda) = \begin{pmatrix} \frac{\lambda}{\eta^2} & -\frac{1}{\eta} \\ -\frac{1}{\eta} & \psi'(\lambda) \end{pmatrix} \quad (5)$$

45 where  $\psi$  is the digamma function.

46 It is sometimes convenient to perform a change of parameterization in order to have a diagonal  
 47 form for the metric. The next proposition is of common use and allows the computation of a pullback  
 48 metric in local coordinates:

**Proposition 4.** *Let  $\mathcal{M}$  be a smooth manifold and  $(\mathcal{N}, g)$  be a smooth Riemannian manifold. For a smooth diffeomorphism  $f: \mathcal{M} \rightarrow \mathcal{N}$ , the pullback metric  $f^*g$  has matrix expressed in local coordinates at the point  $m \in \mathcal{M}$  by:*

$$J_f^t(m)G(f(m))J_f(m) \quad (6)$$

49 with  $J_f(m)$  the jacobian matrix of  $f$  at  $m$  and  $G(n)$  the matrix of the metric  $g$  at  $n \in \mathcal{N}$ .

Performing the change of parameterization:  $f: (\mu, \beta) \mapsto (\eta = \beta/\mu, \lambda = \beta)$  yields:

$$J_f(\mu, \beta) = \begin{pmatrix} -\frac{\mu}{\beta^2} & \frac{1}{\beta} \\ 0 & 1 \end{pmatrix}$$

Using prop. 4 then gives for the pullback metric matrix:

$$G(\mu, \beta) = \begin{pmatrix} \frac{\beta}{\mu^2} & 0 \\ 0 & \psi(\beta)' - \frac{1}{\beta} \end{pmatrix}.$$

50 The information geometry of the gamma distribution is studied in details in [6], with explicit  
 51 calculations of the Christoffel symbols and the geodesic equation.

### 52 3. The geometry of the generalized gamma manifold

53 While the gamma distribution is well suited to study departure to full randomness has pointed  
 54 out in [6], it is not general enough in many applications. In particular, the Weibull distribution, that  
 55 also generalizes the exponential distribution is not a gamma distribution. A more general family was  
 56 thus introduced, by adding a power term.

**Definition 3.** *The generalized gamma distribution is the probability measure on  $\mathbb{R}^+$  with density relative to the Lebesgue measure given by:*

$$p(x; \alpha, \lambda, \beta) = \frac{\beta x^{\beta\lambda-1}}{\alpha^{\beta\lambda}\Gamma(\lambda)} e^{-\left(\frac{x}{\alpha}\right)^\beta}, \quad x > 0 \quad (7)$$

57 where  $\alpha > 0, \lambda > 0, \beta > 0$ .

58 Due to the exponent  $\beta$ , the generalized gamma distribution does not define a natural exponential  
 59 family. However, letting  $\beta$  fixed, the mapping  $\Phi_\beta: x \mapsto x^\beta$  is a diffeomorphism of  $\mathbb{R}^+$  to itself, and  
 60 the image density of  $p(\alpha, \lambda, \beta)$  under  $\Phi_\beta$  is a gamma density with parameters  $(\alpha^\beta, \lambda)$ . For any  $\kappa > 0$ ,

61 the submanifold  $\beta = \kappa$  of the generalized gamma manifold is diffeomorphic to the gamma manifold.  
 62 Using the invariance of the Fisher metric under diffeomorphisms, the induced metric on the above  
 63 submanifold can be obtained.

**Proposition 5.** *Let  $\kappa > 0$  be a fixed real number. The induced Fisher metric  $G_\kappa$  on the submanifold  $(\alpha, \lambda, \kappa)$  of the generalized gamma manifold is given in local coordinates by:*

$$G_\kappa(\alpha, \lambda) = \begin{pmatrix} \frac{\lambda\kappa^2}{\alpha^2} & -\frac{\kappa}{\alpha} \\ -\frac{\kappa}{\alpha} & \psi'(\lambda) \end{pmatrix}.$$

**Proof.** In local coordinates  $(\alpha^\kappa, \lambda)$ , the Fisher metric of a gamma distribution manifold  $(\alpha^\kappa, \lambda)$  is

$$G_\kappa(\alpha^\kappa, \lambda) = \begin{pmatrix} \frac{\lambda}{\alpha^{2\kappa}} & -\frac{1}{\alpha^\kappa} \\ -\frac{1}{\alpha^\kappa} & \psi'(\lambda) \end{pmatrix}.$$

The Jacobian matrix of the transformation  $(\alpha, \lambda) \rightarrow (\alpha^\kappa, \lambda)$  is the matrix  $J = \text{diag}(\kappa\alpha^{\kappa-1}, 1)$  and the change of parametrization yields:

$$G_\kappa(\alpha, \lambda) = J^t G_\kappa(\alpha^\kappa, \lambda) J.$$

64 The Fisher metric on the submanifold  $(\alpha, \lambda, \kappa)$  is directly obtained from the invariance by using the  
 65 diffeomorphism  $\Phi_\beta: x \mapsto x^\beta$ .  $\square$

**Proposition 6.** *In local coordinates, the fisher information metric of the generalized gamma manifold is given by:*

$$G(\alpha, \lambda, \beta) = \begin{pmatrix} \frac{\beta^2\lambda}{\alpha^2} & -\frac{\beta}{\alpha} & \frac{-\lambda\psi(\lambda)-1}{\alpha} \\ -\frac{\beta}{\alpha} & \psi'(\lambda) & -\frac{\psi(\lambda)}{\beta} \\ \frac{-\lambda\psi(\lambda)-1}{\alpha} & -\frac{\psi(\lambda)}{\beta} & \frac{\lambda\psi(\lambda)^2+2\psi(\lambda)+\lambda\psi'(\lambda)+1}{\beta^2} \end{pmatrix} \quad (8)$$

66 **Proof.** The  $2 \times 2$  submatrix corresponding to local coordinates  $\alpha, \lambda$  has already been obtained in prop.  
 67 5. The remaining terms can be computed by differentiating the log likelihood function twice, but an  
 68 alternative will be given below in a more general setting.  $\square$

The usual definition of the generalized gamma distribution 3 does stems from the gamma one by a simple change of variable, thus making some computation less natural. Starting with the above diffeomorphism  $\Phi_\beta$  and applying it to a gamma distribution yields an equivalent, but more intuitive form. Furthermore, it is advisable to express the gamma density as a natural exponential family distribution:

$$p(x; \eta, \lambda) = \frac{\eta^\lambda x^{\lambda-1} e^{-\eta x}}{\Gamma(\lambda)}, \quad x > 0,$$

69 where  $\lambda > 0, \eta > 0$  are the natural parameters of the distribution.

**Definition 4.** *The generalized gamma distribution on  $\mathbb{R}^+$  is the probability measure with density:*

$$p(x; \eta, \lambda, \beta) = \frac{\beta \eta^\lambda x^{\beta\lambda-1} e^{-\eta x^\beta}}{\Gamma(\lambda)}, \quad x > 0,$$

70 with  $\eta > 0, \lambda > 0$  and  $\beta > 0$ .

Due the the invariance by diffeomorphism property of the Fisher information metric, the induced metric on the submanifolds  $\beta = \text{cte}$  is independent of  $\beta$ , and is exactly the one of the gamma manifold, here given by:

$$g(\eta, \lambda) = \begin{pmatrix} \frac{\lambda}{\eta^2} & -\frac{1}{\eta} \\ -\frac{1}{\eta} & \psi'(\lambda) \end{pmatrix}. \quad (9)$$

An important fact about the family of diffeomorphisms  $\Phi_\beta$  is the group property  $\Phi_{\beta_1} \circ \Phi_{\beta_2} = \Phi_{\beta_1\beta_2}$ . It turns out that all the computation can be conducted in a general Lie group setting, as detailed below. Let  $p_\theta, \theta \in \Theta$ , be a parameterized family of probability densities defined on an open subset  $U$  of  $\mathbb{R}^n$  and let  $G$  be a Lie group action on  $U$  by diffeomorphisms preserving orientation. For any  $g$  in  $G$  and  $\theta$  in  $\Theta$ , the image density  $\tilde{p}_{g,\theta}$  under the diffeomorphism  $x \in U \mapsto \zeta(g, x) = g.x$  is given by:

$$\forall x \in U, \tilde{p}_{g,\theta}(x) = p_\theta(\zeta(g, x)) |\partial_2 \zeta(g, x)|.$$

Note that, in this paper, we consider increasing monotone diffeomorphisms. For simplicity of calculus, the absolute value may be remove in the above expression. Denoting  $\tilde{l}(x, \theta, g)$  the log-likelihood of  $\tilde{p}_{g,\theta}(x)$  and  $l(x, \theta)$  the one of  $p_\theta(x)$ , it comes, by obvious computation:

$$\forall x \in U, \tilde{l}(x, \theta, g) = l(\zeta(g, x), \theta) + \log \partial_2 \zeta(g, x).$$

71 Throughout the document, the symbol  $\partial_i$  stands for the partial derivative with respect to the  $i$ -th  
72 variable. Higher order derivatives are written similarly as  $\partial_{i\dots i j\dots j\dots}$  by repeating the variable  $k$  times to  
73 indicate a partial derivative of order  $k$ .

**Proposition 7.** For any  $x \in U, g \in G$ :

$$\partial_1 \tilde{\zeta}(g, x) = \partial_1 \zeta(e, \zeta(g, x)) T_g R_{g^{-1}}$$

74 where  $e$  is the identity of  $G$  and  $R_g$  is the right translation mapping  $h \in G \mapsto R_g.h = h.g$ .

**Proof.** Since  $\zeta$  comes from a group action:

$$\zeta(h, \zeta(g, x)) = \zeta(h.g, x).$$

Then, taking the derivative with respect to  $h$  at identity:

$$\partial_1 \tilde{\zeta}(e, \zeta(g, x)) = \partial_1 \zeta(g, x) T_e R_g.$$

75 Since  $T_e R_g T_g R_{g^{-1}} = Id$  by the chain rule, the claimed result is proved.  $\square$

76 This property allows to compute the Fisher information metric in a convenient way.

**Proposition 8.** The element  $G_{g,\theta}$  of the Fisher metric of  $\tilde{p}_{g,\theta}$  is given by:

$$- \int_U \partial_{12} l(x, \theta) \partial_1 \tilde{\zeta}(e, x) p_\theta(x) dx T_g R_{g^{-1}},$$

**Proof.** Since:

$$\tilde{l}(x, \theta, g) = l(\zeta(g, x), \theta) + \log \partial_2 \zeta(g, x),$$

it comes:

$$\partial_2 \tilde{l}(x, \theta, g) = \partial_2 l(\zeta(g, x), \theta)$$

and thus:

$$\partial_{23} \tilde{l}(x, \theta, g) = \partial_{12} l(\zeta(g, x), \theta) \partial_1 \tilde{\zeta}(g, x).$$

Now, using prop. 7:

$$\partial_{23}\tilde{l}(x, \theta, g) = \partial_{12}l_\theta(\zeta(g, x), \theta)\partial_1\zeta(e, \zeta(g, x))T_gR_{g^{-1}}.$$

Taking the expectation with respect to  $\tilde{p}_{g,\theta}$  yields:

$$E[\partial_{23}] = \int_U \partial_{12}l(\zeta(g, x), \theta)\partial_1\zeta(e, \zeta(g, x))\tilde{p}_{g,\theta}(x)dx T_gR_{g^{-1}}$$

77 and the result follows by the change of variable  $y = \zeta(g, x)$ .  $\square$

The case of the elements  $G_{g,g}$  is a little bit more complex, due to the non vanishing extra term in the log-likelihood  $\tilde{l}(x, \theta, g)$ . Taking the first derivative with respect to  $g$  yields:

$$\forall x \in U, \partial_3\tilde{l}(x, \theta, g) = \partial_1l(\zeta(g, x), \theta)\partial_1\zeta(g, x) + \frac{\partial_{12}\zeta(g, x)}{\partial_2\zeta(g, x)}.$$

78 The second term in the right hand side can be further simplified using the next proposition, that is a  
79 direct consequence of prop. 7.

**Proposition 9.** For any  $\theta \in \Theta, g \in G, x \in U$ :

$$\partial_{12}\zeta(e, \zeta(g, x))\partial_2\zeta(g, x) = \partial_{12}\zeta(g, x) T_eR_g.$$

Applying it to the log-likelihood derivative and using again 7 yields:

$$\forall x \in U, \partial_3\tilde{l}(x, \theta, g) = (\partial_1l(\zeta(g, x), \theta)\partial_1\zeta(e, \zeta(g, x)) + \partial_{12}\zeta(e, \zeta(g, x))) T_gR_{g^{-1}}.$$

**Proposition 10.** The element  $G_{g,g}$  of the Fisher metric of  $\tilde{p}_{g,\theta}$  is given in matrix form by:

$$T_gR_{g^{-1}} \int_U h_{g,\theta}(x)^T h_{g,\theta}(x) p_\theta(x) dx T_gR_{g^{-1}}$$

with:

$$h_{g,\theta}(x) = \partial_1l(x, \theta)\partial_1\zeta(e, x) + \partial_{12}\zeta(e, x).$$

**Proof.** Starting with the definition:

$$G_{g,g} = E[(\partial_3\tilde{l})^T (\partial_3\tilde{l})]$$

80 the result follows after the change of variable  $y = \zeta(g, x)$  in the expectation.  $\square$

81 An important corollary of 8 and 10 is that the Fisher metric is right invariant with respect to the  
82 group action.

83 Propositions 8 and 10 allow to compute the coefficients  $g_{\eta\beta}, g_{\lambda\beta}, g_{\beta\beta}$  in the Fisher metric, thus  
84 yielding the next proposition.

**Proposition 11.** *The Fisher information matrix in natural coordinates has coefficients:*

$$\begin{aligned} g_{\eta\eta} &= \frac{\lambda}{\eta^2} \\ g_{\eta\lambda} &= -\frac{1}{\eta} \\ g_{\lambda\lambda} &= \psi'(\lambda) \\ g_{\eta\beta} &= \frac{\lambda}{\eta\beta} (\psi(\lambda+1) - \log \eta) \\ g_{\lambda\beta} &= \frac{1}{\beta} (\log \eta - \psi(\lambda)) \\ g_{\beta\beta} &= \frac{1}{\beta^2} \left[ 1 + \lambda \log^2 \eta - 2\lambda\psi(\lambda+1) \log \eta + \lambda\psi^2(\lambda+1) + \lambda\psi'(\lambda+1) \right] \end{aligned}$$

Recalling that the Christoffel symbols of the first kind for the Levi-Civita connection are obtained using the formula:

$$\Gamma_{kij} = \frac{1}{2} \left( \partial_i g_{jk} + \partial_j g_{ik} - \partial_k g_{ij} \right)$$

one can obtain them as:

$$\begin{aligned} \Gamma_{111} &= -\frac{\lambda}{\eta^3} & \Gamma_{211} &= \frac{1}{2\eta^2} & \Gamma_{311} &= \frac{\lambda(-1+\log \eta - \psi(\lambda+1))}{\eta^2\beta} \\ \Gamma_{121} &= \Gamma_{211} = \Gamma_{112} & \Gamma_{221} &= \Gamma_{212} = 0 & \Gamma_{321} &= \Gamma_{312} = \frac{1-\log \eta + \psi(\lambda+1) + \lambda\psi'(\lambda+1)}{2\eta\beta} \\ \Gamma_{122} &= 0 & \Gamma_{222} &= \frac{1}{2}\psi''(\lambda) & \Gamma_{322} &= -\frac{\psi'(\lambda)}{\beta} \end{aligned} \quad (10)$$

$$\begin{aligned} \Gamma_{131} &= \Gamma_{113} = 0 \\ \Gamma_{231} &= \Gamma_{213} = \frac{1+\log \eta - \psi(\lambda+1) - \lambda\psi'(\lambda+1)}{2\eta\beta} \\ \Gamma_{331} &= \Gamma_{313} = \frac{\lambda(\log \eta - \psi(\lambda+1))}{\eta\beta^2} \\ \Gamma_{132} &= \Gamma_{123} = \frac{-1-\log \eta + \psi(\lambda+1) + \lambda\psi'(\lambda+1)}{2\eta\beta} \\ \Gamma_{232} &= \Gamma_{223} = 0 \\ \Gamma_{332} &= \Gamma_{323} = \frac{\psi'(\lambda+1)(1-2\lambda \log \eta) - 2\psi(\lambda+1)(\log \eta - \lambda\psi'(\lambda+1)) + \log^2 \eta + \psi(\lambda+1)^2 + \lambda\psi''(\lambda+1)}{2\beta^2} \\ \Gamma_{133} &= 0 \\ \Gamma_{233} &= -\frac{-2\psi(\lambda+1)(\log \eta - \lambda\psi'(\lambda+1)) + \psi'(\lambda+1)(1-2\lambda \log \eta) + \log \eta(\log \eta + 2) + \psi(\lambda+1)^2 - 2\psi(\lambda) + \lambda\psi''(\lambda+1)}{2\beta^2} \\ \Gamma_{333} &= -\frac{\lambda \log^2 \eta + \lambda(-2 \log \eta \psi(\lambda+1) + \psi(\lambda+1)^2 + \psi'(\lambda+1)) + 1}{\beta^3} \end{aligned} \quad (11)$$

#### 85 4. The gamma submanifold

86 The submanifolds  $\beta = \text{cte}$  of the generalized gamma manifold are all isometric to the gamma  
87 manifold. This section is dedicated to the study of their properties using the Gauss-Codazzi equations.  
88 In the sequel, the generalized gamma manifold will be denoted by  $M$  while  $N_\kappa$ ,  $\kappa > 0$  will stand for  
89 the embedded submanifold  $\beta = \kappa$ .

**Proposition 12.** *The normal bundle to  $N_\kappa$  is generated at  $(\eta, \lambda)$  on the gamma submanifold by the vector:*

$$n(\eta, \lambda) = (-\eta(\lambda\psi'(\lambda)(\psi(\lambda+1) - \log(\eta)) + \log(\eta) - \psi(\lambda)), -1, \kappa(\lambda\psi'(\lambda) - 1))$$

**Proof.** The matrix of the Fisher metric at  $(\eta, \lambda, \beta)$  can be written in block form as:

$$G(\eta, \lambda, \beta) = \begin{pmatrix} g(\eta, \lambda) & v \\ v^t & g_{\beta\beta} \end{pmatrix}$$

with:

$$g(\eta, \lambda) = \begin{pmatrix} \frac{\lambda}{\eta^2} & -\frac{1}{\eta} \\ -\frac{1}{\eta} & \psi'(\lambda) \end{pmatrix}$$

and

$$v = \begin{pmatrix} \frac{\lambda}{\eta\beta}(\psi(\lambda+1) - \log \eta) \\ \frac{1}{\beta}(\log \eta - \psi(\lambda)) \end{pmatrix}$$

Any multiple of the vector:

$$(-g(\eta, \lambda)^{-1}v, 1)$$

is normal to the tangent space to the submanifold  $N_\kappa$ . The result follows by simple computation.  $\square$

Let  $\nabla$  be the levi-civita connection of the gamma manifold and  $\bar{\nabla}$  that of the generalized gamma. It is well known [7] (pp 60-63) that these two connections are related by the Gauss formula:

$$\forall X, Y \in TN_\kappa, \bar{\nabla}_X Y = \nabla_X Y + \mathcal{B}(X, Y) \quad (12)$$

where  $\mathcal{B}$  is a symmetric bilinear form with values in the normal bundle. Letting  $n = n^i e_i$  with  $e_1 = \partial_\eta, e_2 = \partial_\lambda, e_3 = \partial_\beta$ , it comes, with  $i, j = 1 \dots 2$ :

$$g(\bar{\nabla}_{e_i} e_j, n) = n^k \bar{\Gamma}_{kij} = g(\nabla_{e_i} e_j, n) + g(\mathcal{B}(e_i, e_j), n). \quad (13)$$

Since  $\mathcal{B}$  takes its values in the normal bundle, it exists a smooth real value mapping  $a_{ij}, i, j = 1 \dots 2$  such that  $\mathcal{B}(e_i, e_j) = a_{ij}n$ . The equation 13 yields:

$$a_{ij} = \frac{n^k \bar{\Gamma}_{kij}}{g(n, n)}. \quad (14)$$

From [7] (p 63), the sectional curvature  $\bar{K}(e_1, e_2)$  of  $M$  can be obtained from the one  $K(e_1, e_2)$  of  $N_\kappa$  as:

$$\bar{K}(e_1, e_2) = K(e_1, e_2) + \frac{g(\mathcal{B}(e_1, e_2), \mathcal{B}(e_1, e_2)) - g(\mathcal{B}(e_1, e_1), \mathcal{B}(e_2, e_2))}{g(e_1, e_1)g(e_2, e_2) - g(e_1, e_2)^2} \quad (15)$$

or:

$$\bar{K}(e_1, e_2) = K(e_1, e_2) + g(n, n) \frac{a_{12}^2 - a_{11}a_{22}}{g_{11}g_{22} - g_{12}^2}. \quad (16)$$

Using the expressions if the Christoffel symbols and the metric, the coefficients  $a_{11}, a_{12}, a_{22}$  can be computed as:

$$a_{11} = \frac{2\lambda(1 - \lambda\psi'(\lambda)) + 1}{2\eta^2 D} \quad (17)$$

$$a_{12} = \frac{\lambda^2\psi'(\lambda)^2 - \psi'(\lambda) - 1}{2\eta D} \quad (18)$$

$$a_{22} = \frac{\psi'(\lambda)(1 - \lambda\psi'(\lambda)) - \psi''(\lambda)/2}{D} \quad (19)$$

with:

$$D = g(n, n) = (\lambda\psi'(\lambda) - 1)(\psi'(\lambda)(\lambda^2\psi'(\lambda) - 1) - 1).$$

Finally:

$$g(n, n) \frac{a_{12}^2 - a_{11}a_{22}}{g_{11}g_{22} - g_{12}^2} = F(\lambda)/G(\lambda) \quad (20)$$

with:

$$F(\lambda) = \lambda^4 \psi'(\lambda)^4 - 2\lambda^2(2\lambda + 1)\psi'(\lambda)^3 + (6\lambda^2 + 2\lambda + 1)\psi'(\lambda)^2 - 2\lambda(\lambda\psi''(\lambda) + 2)\psi'(\lambda) + (2\lambda + 1)\psi''(\lambda) + 1$$

and:

$$G(\lambda) = 4(\lambda\psi'(\lambda) - 1)^2 (\psi'(\lambda) (\lambda^2\psi'(\lambda) - 1) - 1).$$

91 **Proposition 13.** *The term  $a_{12}^2 - a_{11}a_{22}$  is strictly positive.*

**Proof.** Using the expressions of the coefficients:

$$a_{12}^2 - a_{11}a_{22} = \frac{1}{4\eta^2 D^2} (A(\lambda) + B(\lambda)C(\lambda))$$

with:

$$\begin{aligned} A(\lambda) &= (\lambda^2\psi'(\lambda)^2 - \psi'(\lambda) - 1)^2 \\ B(\lambda) &= 2\lambda(1 - \lambda\psi'(\lambda)) + 1 \\ C(\lambda) &= 2\psi'(\lambda)(-1 + \lambda\psi'(\lambda)) + \psi''(\lambda). \end{aligned}$$

The  $\psi'$  function satisfies the next inequality [8]:

$$\frac{1}{\lambda} + \frac{1}{2\lambda^2} < \psi'(\lambda) < \frac{1}{\lambda} + \frac{1}{\lambda^2}$$

from which it comes:

$$-\frac{1}{2\lambda} > 1 - \lambda\psi'(\lambda) > -\frac{1}{\lambda}$$

and in turn:

$$0 > B(\lambda) > -1.$$

To obtain the sign of  $C(\lambda)$ , a different bound is needed for the polygamma function. Again from [8]:

$$\frac{(k-1)!}{(x+1)^k} + \frac{k!}{x^{k+1}} < |\psi^{(k)}| < \frac{(k-1)!}{(x+1/2)^k} + \frac{k!}{x^{k+1}}, \quad k \geq 1. \quad (21)$$

Using the inequality 21, it comes:

$$\frac{\lambda+1}{\lambda(2\lambda+1)} < \lambda\psi'(\lambda) - 1$$

so that:

$$\left(\frac{1}{\lambda+1/2} + \frac{1}{\lambda^2}\right) \left(\frac{\lambda+1}{\lambda(2\lambda+1)}\right) < \psi'(\lambda)(-1 + \lambda\psi'(\lambda)).$$

Using again 21 with  $k = 2$  yields finally:

$$C(\lambda) < -\frac{2}{\lambda^2(1+2\lambda)^2}.$$

92 Since both  $B(\lambda)$  and  $C(\lambda)$  are strictly negative,  $A(\lambda) + B(\lambda)C(\lambda)$  is strictly positive as claimed.  $\square$

**Proposition 14.** *The sectional curvature of the generalized gamma manifold in the  $(e_1, e_2)$  satisfies:*

$$\bar{K}(e_1, e_2) \xrightarrow{\lambda \rightarrow 0^+} \frac{12 - \pi^2}{2(\pi^2 - 6)}.$$

**Proof.** The sectional curvature of the gamma manifold satisfies [6]:

$$K(e_1, e_2) \xrightarrow{\lambda \rightarrow 0^+} -\frac{1}{2}.$$

It is thus only needed to estimate the limit of (20) when  $\lambda \rightarrow 0^+$ . The asymptotics of the polygamma functions at 0 are given by:

$$\begin{aligned}\psi'(\lambda) &= \frac{1}{\lambda^2} + \psi'(1) + o(1), \\ \psi''(\lambda) &= -\frac{2}{\lambda^3} + \psi''(1) + o(1).\end{aligned}$$

The term:

$$\begin{aligned}F(\lambda) &= \lambda^4 \psi'(\lambda)^4 - 2\lambda^2(2\lambda + 1)\psi'(\lambda)^3 + (6\lambda^2 + 2\lambda + 1)\psi'(\lambda)^2 \\ &\quad - 2\lambda(\lambda\psi''(\lambda) + 2)\psi'(\lambda) + (2\lambda + 1)\psi''(\lambda) + 1\end{aligned}$$

can thus be approximated by:

$$\begin{aligned}&\left( \pi^8 x^6 - 24\pi^6 x^5 + 12\pi^6 x^4 + 216\pi^4 x^4 - 432\pi^2 x^4 \psi''(1) - 360\pi^4 x^3 - 864\pi^2 x^3 + \right. \\ &\quad \left. 2592x^3 \psi''(1) + 36\pi^4 x^2 + 2592\pi^2 x^2 + 1296x^2 - 1296x^2 \psi''(1) - 864\pi^2 x - 5184x + 2592 \right) / (1296x^2)\end{aligned}$$

and the term :

$$G(\lambda) = 4(\lambda\psi'(\lambda) - 1)^2 \left( \psi'(\lambda) (\lambda^2\psi'(\lambda) - 1) - 1 \right).$$

is approximated by:

$$\frac{(\pi^2 x^2 - 6x + 6)^2 (\pi^4 x^2 + 6\pi^2 - 36)}{324x^2}$$

Finally, the quotient  $F(\lambda)/G(\lambda)$  is equal at  $\lambda = 0$  to

$$\frac{3}{\pi^2 - 6}$$

93 and the result follows by summation with  $-1/2$ .  $\square$

94 It is conjectured that the sectional curvature of the generalized gamma manifold in the directions  
95  $\partial_\eta, \partial_\lambda$  is strictly positive, bounded from above by  $1/2$  as it appears to be the case numerically.

## 96 5. Medical imaging application

97 Magnetic Resonance Imaging (MRI) seeks to identify, localize and measure different parts  
98 of the anatomy of the central nervous system, and has been demonstrated as a valid marker of  
99 neurodegenerative diseases such as Alzheimer's disease, the most common cause of dementia [9–11].  
100 Indeed, brain atrophy measured by structural MRI has been proposed as a surrogate marker for the  
101 early diagnosis of Alzheimer's disease [12,13].

102 Many of these studies limited their work by using central tendency measures such as the mean or  
103 the median and more recent ones used histogram-analysis [14,15] in order to represent a biomarker  
104 rather than using the biomarker probability distribution of the whole brain or of specific tissues. In this  
105 section, we present one of the possible applications of information geometry on manifold of probability  
106 distributions and demonstrate the use of probability distributions in the context of the classification of  
107 the Alzheimer's disease population.

### 108 5.1. Study set-up and design

109 Data used in the preparation of this paper were obtained from the Alzheimer’s disease  
 110 Neuroimaging Initiative (ADNI) database. ADNI is a project that has been initiated in 2004 by the  
 111 National Institute on Aging (NIA), the National Institute of Biomedical Imaging and Bioengineering  
 112 (NIBIB) and the Food and Drug Administration (FDA), whose principal investigator is Dr. Michael  
 113 Weiner. ADNI provides all data without embargo to all scientists in the world. The aim of the project  
 114 is the development of clinical, genetic, biochemical or imaging biomarkers for the early diagnosis and  
 115 follow-up of Alzheimer’s disease. For up-to-date information, see [ADNI website](#).

### 116 5.2. Participants

117 Our study is based on a part of ADNI population. Indeed, the initial subjects were not age- and  
 118 sex-matched and our procedure consisted in randomly selecting subjects. In addition, some of the  
 119 subjects were excluded because of a low diagnosis reliability (according to ADNI criteria) and others  
 120 because of unsuccessful cortical thickness measurement due to poor image quality. The resulting  
 121 population is composed of 143 subjects; 71 healthy controls (HC) subjects and 72 Alzheimer’s disease  
 122 (AD) patients whose demographic data are presented in Table 1.

### 123 5.3. MRI Acquisition

124 MRI volumes were downloaded from ADNI1 (i.e. ADNI first study). All the MR scans  
 125 are T1-weighted MR images and were acquired on a 1.5 Tesla scanner. For each subject, we  
 126 only used the MRI scan from the baseline visit and the ones that were acquired according to  
 127 3D MP-RAGE (Magnetization -Prepared Rapid Acquisition Gradient Echo) sequence. The 3D  
 128 MP-RAGE sequence was used with the following protocol parameters: slice width = 1.2mm;  
 129 echo time (TE)=3.61ms; repetition time (TR)=3000 ms; flip angle=8deg; matrix size=192x192;  
 130 slice number=160-170; FOV=250mm; pixel size=1.25mmx1.25mm. The MPRAGE images are  
 131 considered the best in the quality ratings and have undergone gradwarping, intensity correction,  
 132 and have been scaled for gradient drift using the phantom data.

### 133 5.4. Cortical thickness measurement and distribution

134 Cortical thickness was chosen as the MRI biomarker because of its ability to quantify  
 135 morphological alterations of the cortical mantle in early stage of AD. Cortical Thickness (CTh) was  
 136 measured using the Matlab Toolbox CorThiZon [16] and computed on the entire cortical ribbon using  
 137 a Laplace’s-equation-based algorithm as described by Jones *et al* [17]. Thus, a 3D cortical thickness  
 138 map was obtained.

139 We applied the method of moments previously described to estimate the three generalized gamma  
 140 parameters ( $\alpha, \lambda, \beta$ ) and thus we obtained the CTh distribution.

**Table 1.** Demographic and clinical characteristics of the study population

	HC (n=71)	AD (n=72)	p-value
Age (years)	76.1 ± 5.6	77.4 ± 5.5	0.17
Sex (F/M)	38 / 33	41 / 31	0.20
MMSE	29 ± 0.9	23.2 ± 2.1	<0.001

Plus-minus values are means ± standard deviation. All p-values are based on ANOVA test, apart from Sex, which is based on Chi-square tests ( $\alpha < 0.05$ ). Abbreviations: HC, Healthy Control; AD, Alzheimer’s disease patients; MMSE, Mini Mental State Examination.

### 141 5.5. Clustering Based on Distribution Similarity

142 Clustering, also called unsupervised classification, has been extensively studied for years in  
 143 many fields, such as data mining, pattern recognition, image segmentation and bioinformatics. This  
 144 technique is used primarily to segment or classify a database or extract knowledge to attempt to  
 145 identify subsets of data that are difficult to distinguish. The aim is to group data sets in a way that the  
 146 intra-cluster similarity is maximized while the inter-cluster similarity is minimized. Three principal  
 147 categories of clustering exist in literature, namely partitioning clustering, hierarchical clustering and  
 148 density-based clustering.

In our study, the experiments were conducted using partitioning k-medoids algorithm [18], that we extended using an approximate geodesic distance that is computed in two steps.

Let  $p(\eta_2, \lambda_2, \beta_2), p(\eta_1, \lambda_1, \beta_1)$  be two generalized gamma densities. The energy  $E_1$  of the path  $t \in [0, 1] \mapsto \gamma_\beta(t) = (\eta_1, \lambda_1, (1-t)\beta_1 + t\eta_2)$  is computed using the formula:

$$E_1 = (\beta_2 - \beta_1)^2 \int_0^1 g_{\beta\beta}(\gamma_\beta(t)) dt$$

149 Then the energy  $E_2$  of the path joining  $p(\eta_1, \lambda_1, \beta_1)$  and  $p(\eta_2, \lambda_2, \beta_2)$  is computed on the gamma  
 150 submanifold only. The overall distance is then taken to be  $\sqrt{E_1 + E_2}$ . Using this approximate distance  
 151 avoids circumvent numerical instabilities resulting from the positive curvature of the generalized  
 152 gamma manifold in the plane  $\partial_\eta, \partial_\lambda$  and yields a faster algorithm.

153 The K-medoids approach, as all clustering algorithm, tries to organize data into  $K$  clusters, to do  
 154 so the method consists of two phases, the building phase and the swapping phase. The building phase  
 155 consists on selecting the initial  $k$  representatives (i.e. medoids) at random. Non-selected objects are  
 156 assigned to the most similar representative according to geodesic distance. Then, in the swapping  
 157 phase, we iteratively replace representatives by non-representative objects (see algorithm 1).

---

#### Algorithm 1 Distribution based K-medoids algorithm

---

1. **Initialization:** Select randomly  $k$  distributions as the initial representative objects (i.e. k-medoids)
  2. **Repeat**
    - i. Calculate the geodesic distance between each medoid  $m$  and the remaining data objects
    - ii. Assign the non representative object  $o_i$  to the closest medoid  $m$  (i.e. smallest geodesic distance)
    - iii. Compute the total cost  $S$  of swapping the medoid  $m$  with  $o_i$ ; the total cost is defined to be the sum of the squared errors SSE of the resulting clustering
    - iv. If  $S < 0$ , then swap  $m$  with  $o_i$  to form the new set of medoids
  3. **Until**  
Convergence criterion is satisfied (i.e. no change in the medoids or in total swapping cost)
- 

158 The K-medoids algorithm is chosen instead of k-means algorithm for mainly two reasons:  
 159 It minimizes a sum of pairwise dissimilarities instead of a sum of squared Euclidean distances.  
 160 Consequently it is more robust to noise and outliers as compared to k-means. Moreover, k-means  
 161 represent each cluster by the mean of all objects in this cluster, while k-medoids use an actual object in  
 162 a cluster as its representative and since the objects in our case are probability distributions; it was more  
 163 efficient to proceed with the k-medoids method [19].

## 165 5.6. Results

The quality of the clustering results was assessed using an external evaluation measure, called *Purity*. The external clustering measures are used to assess how well clusters matched up with real labels. In order to compute the evaluation measure *Purity*, each cluster is assigned to the class which is most frequent in the cluster, and then the accuracy of this assignment is measured by counting the number of correctly assigned objects and dividing by the total number of objects. It is the percent of the total number of objects that were classified correctly.

$$\text{Purity} = \frac{1}{N} \sum_{i=1}^k \max_j |c_i \cap t_j| \quad (22)$$

166 where  $N$  is the number of objects,  $k$  is the number of clusters,  $c_i$  is the number of objects in the  $i$ -th  
 167 cluster of the clustering solution, and  $t_j$  the number of objects in the  $j$ -th cluster of the groundtruth  $c_i$   
 168 and  $|c_i \cap t_j|$  is the number of objects in both the  $i$ -th cluster of the clustering solution and  $j$ -th cluster of  
 169 the groundtruth. Figure 1 summarizes the approach.

170 In our case, the aim was to assess how accurately our approach would group AD patients and  
 171 HC subjects. Thus, we have chosen  $k = 2$  as cluster number in the k-medoids algorithm, one cluster  
 172 would represent the AD patients and the other the HC subjects. These clusters are compared with the  
 173 true label data using the *Purity* measure. We obtained **Purity=0.84**, meaning that the two clusters of  
 174 the distribution based k-medoids algorithm match up with 84% of the real labels.

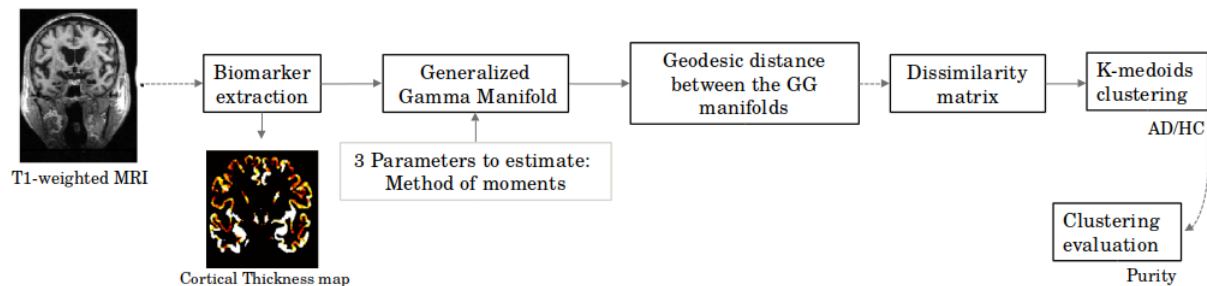


Figure 1. General scheme of the proposed approach

## 175 5.7. Discussion

176 The distribution based K-medoids algorithm obtains accurate classification of the Alzheimer's  
 177 disease population (Purity = 84%). Indeed, information geometry offers suitable tools that allows the  
 178 proper use of probability distribution, which increase significantly the performance of the disease  
 179 classification compared to classical approaches [10]. Thus, we can consider that this approach is a  
 180 powerful aid to study neurological diseases.

181 **Author Contributions:** F. Nicol and S. Puechmorel have contributed equally to the geometry of the generalized  
 182 gamma manifold. S. Rebbah has written the part on medical applications.

183 **Funding:**

184 **Acknowledgments:** This work was supported by the Fondation pour la Recherche Medicale (FRM grant number  
 185 ECO20160736068 to S.R).

186 **Conflicts of Interest:** 'The authors declare no conflict of interest

## 187 Abbreviations

188 The following abbreviations are used in this manuscript:

189

AD Alzheimer's Disease  
 CTh Cortical Thickness  
 190 HC Healthy Control  
 GG Generalized Gamma  
 MRI Magnetic Resonance Imaging

## 191 References

- 192 1. Stacy, E.W. A Generalization of the Gamma Distribution. The Annals of Mathematical Statistics **1962**,  
 193 33, 1187–1192.
- 194 2. Amoroso, L. Ricerche intorno alla curva dei redditi. Annali di Matematica Pura ed Applicata **1925**,  
 195 2, 123–159.
- 196 3. Crooks, G.E. The Amoroso Distribution. arXiv preprint arXiv:1005.3274 **2010**.
- 197 4. Shima, H. Geometry of Hessian Structures. Geometric Science of Information; Nielsen, F.; Barbaresco, F.,  
 198 Eds.; Springer Berlin Heidelberg: Berlin, Heidelberg, 2013; pp. 37–55.
- 199 5. Duistermaat, J. On Hessian Riemannian structures. Asian journal of mathematics **2001**, 5, 79–91.
- 200 6. Arwini, K.; Dodson, C.; Doig, A.; Sampson, W.; Scharcanski, J.; Felipussi, S. Information Geometry: Near  
 201 Randomness and Near Independence; Information Geometry: Near Randomness and Near Independence,  
 202 Springer, 2008.
- 203 7. Chavel, I. Riemannian Geometry: A Modern Introduction; Cambridge Studies in Advanced Mathematics,  
 204 Cambridge University Press, 2006.
- 205 8. Guo, B.; F., Q.; J.L., Z.; Luo Q.M., journal=Mathematica Clovaca, v.y. Sharp Inequalities for Polygamma  
 206 Functions.
- 207 9. Vemuri, P.; Jack, C.R. Role of structural MRI in Alzheimer's disease. Alzheimer's Research & Therapy  
 208 **2010**, 2, 23. doi:10.1186/alzrt47.
- 209 10. Cuingnet, R.; Gerardin, E.; Tessieras, J.; Auzias, G.; Lehéricy, S.; Habert, M.O.; Chupin, M.; Benali,  
 210 H.; Colliot, O.; Alzheimer's Disease Neuroimaging Initiative. Automatic classification of patients  
 211 with Alzheimer's disease from structural MRI: a comparison of ten methods using the ADNI database.  
 212 NeuroImage **2011**, 56, 766–781. doi:10.1016/j.neuroimage.2010.06.013.
- 213 11. Lama, R.K.; Gwak, J.; Park, J.S.; Lee, S.W. Diagnosis of Alzheimer's Disease Based on Structural MRI Images  
 214 Using a Regularized Extreme Learning Machine and PCA Features. Journal of Healthcare Engineering  
 215 **2017**, 2017. doi:10.1155/2017/5485080.
- 216 12. Pini, L.; Pievani, M.; Bocchetta, M.; Altomare, D.; Bosco, P.; Cavado, E.; Galluzzi, S.; Marizzoni, M.;  
 217 Frisoni, G.B. Brain atrophy in Alzheimer's Disease and aging. Ageing Research Reviews **2016**, 30, 25–48.  
 218 doi:10.1016/j.arr.2016.01.002.
- 219 13. Busovaca, E.; Zimmerman, M.E.; Meier, I.B.; Griffith, E.Y.; Grieve, S.M.; Korgaonkar, M.S.; Williams, L.M.;  
 220 Brickman, A.M. Is the Alzheimer's disease cortical thickness signature a biological marker for memory?  
 221 Brain imaging and behavior **2016**, 10, 517–523. doi:10.1007/s11682-015-9413-5.
- 222 14. Ruiz, E.; Ramírez, J.; Górriz, J.M.; Casillas, J.; Alzheimer's Disease Neuroimaging Initiative.  
 223 Alzheimer's Disease Computer-Aided Diagnosis: Histogram-Based Analysis of Regional MRI Volumes  
 224 for Feature Selection and Classification. Journal of Alzheimer's disease: JAD **2018**, 65, 819–842.  
 225 doi:10.3233/JAD-170514.
- 226 15. Giulietti, G.; Torso, M.; Serra, L.; Spanò, B.; Marra, C.; Caltagirone, C.; Cercignani, M.; Bozzali, M.;  
 227 Alzheimer's Disease Neuroimaging Initiative (ADNI). Whole brain white matter histogram analysis  
 228 of diffusion tensor imaging data detects microstructural damage in mild cognitive impairment and  
 229 alzheimer's disease patients. Journal of magnetic resonance imaging: JMRI **2018**. doi:10.1002/jmri.25947.
- 230 16. Querbes, O.; Aubry, F.; Pariente, J.; Lotterie, J.A.; Démonet, J.F.; Duret, V.; Puel, M.; Berry, I.; Fort, J.C.;  
 231 Celsis, P.; Alzheimer's Disease Neuroimaging Initiative. Early diagnosis of Alzheimer's disease using  
 232 cortical thickness: impact of cognitive reserve. Brain: A Journal of Neurology **2009**, 132, 2036–2047.  
 233 doi:10.1093/brain/awp105.
- 234 17. Jones, S.E.; Buchbinder, B.R.; Aharon, I. Three-dimensional mapping of cortical thickness using Laplace's  
 235 equation. Human Brain Mapping **2000**, 11, 12–32.

- 236 18. Kaufman, L.; Rousseeuw, P. Clustering by means of Medoids. Statistical Data Analysis Based on the  
237 L1-Norm and Related Methods, edited by Y. Dodge, North-Holland **1987**, pp. 405–416.
- 238 19. Soni, K.G.; Patel, D.A. Comparative Analysis of K-means and K-medoids Algorithm on IRIS Data.  
239 International Journal of Computational Intelligence Research **2017**, 13, 899–906.

240 **Sample Availability:** Samples of the compounds ..... are available from the authors.

241 © 2019 by the authors. Submitted to Mathematics for possible open access publication  
242 under the terms and conditions of the Creative Commons Attribution (CC BY) license  
243 (<http://creativecommons.org/licenses/by/4.0/>).